RE-ENTRANT FILTER ANALYSIS YIELDING BROADBAND AND COMPACT DESIGNS

This article presents a more thorough validation of an analysis method of a re-entrant filter and augments the work performed previously on this type of filter.[1] Validation of the analysis was achieved by comparing results with the High Frequency Structure Simulator (HFSS™) and measurements of a prototype unit. The analysis model was improved from previous work[1] by including frequency-dependent microstrip-to-slot line coupling effects, slot line impedance computations and a better capacitive gap model. The analysis method yielded good agreement with measured data and accurate HFSS simulations.

The work presented in this article for the re-entrant filter is a more thorough validation of re-entrant filter analysis results with further enhancements to the transmission line (T-line) model equations. This novel filter topology and an analysis method were first presented in in 1995.[1] A re-entrant filter layout is shown in ***Figure 1***. The analysis circuit model used originally[1] is shown in ***Figure 2***. The circuit used in the analysis is a planar combination of microstrip and slot line transmission lines with capacitive coupling between the microstrip lines, as shown in ***Figure 3***. This combination produces a broadband, highpass, elliptic/pseudo-elliptic function response in a compact geometry. The beauty of incorporating the re-entrant filter geometry in designs is that it lends itself not just to a highpass response, but also to lowpass and bandpass re-

▼ *Fig. 1 The re-entrant filter prototype layout.*

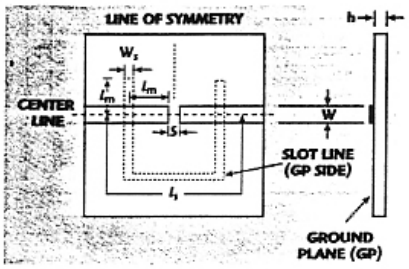

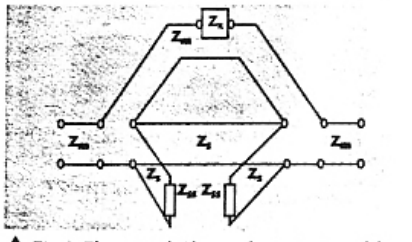

▲ *Fig. 2 The original T-line analysis circuit model.*

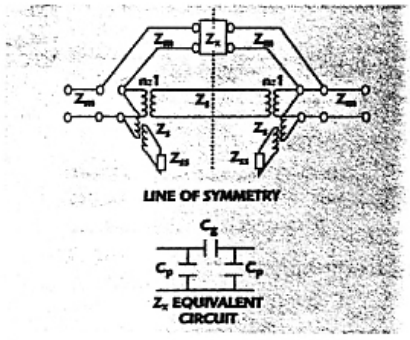

▲ *Fig. 3 The enhanced T-line circuit.*

[Continued on page 22]

LUIS R. AMARO
AND MATTHEW M. RADMANESH
California State University
Northridge, CA

sponses as shown in ***Figures 4*** and ***5***, respectively. A lowpass configuration is achieved by replacing the capacitive element with an inductive element and by selecting the proper microstrip and slot line lengths. The response of the lowpass configuration using a 5 nH inductance could be used alternatively as a band-stop response. A bandpass response also can be achieved by the proper selection of microstrip and slot line lengths.

However, the possibility of realizing a lowpass re-entrant filter appears limited by at least two factors: the availability of inductors in the range of those shown at microwave frequencies, and the short rejection band seen with both the lowpass and bandpass responses. As is the case with distributed element filters, the attenuation does not increase monotonically. By nature, the re-entrant filter is a highpass filter since the coupling between the microstrip and the slot line tends to go to zero as the frequency approaches DC. The selectivity of the filter response can be varied by judicious selection of the capacitive gap and the stub lengths.

The circuit function can be described simply. When current is applied to the microstrip an incident wave flows toward the microstrip-to-slot line transition. The slot line causes a current discontinuity on the ground plane, which causes an electric field to be coupled into the slot line circuit. In the slot line the signal is divided into two traveling waves: a forward and a reverse wave moving away from the junction along the slot line. The reverse wave travels along the slot line short- or open-circuited stub only to be reflected back to interact with the junction once more. The forward-wave signal propagates down the slot line toward the second microstrip-to-slot line transition. This forward signal forms the re-entrant path, which gives the geometry its name.

The re-entrant filter analysis is based on even-/odd-mode analysis[4] and the equations were implemented into MATHCAD.™ The MATHCAD

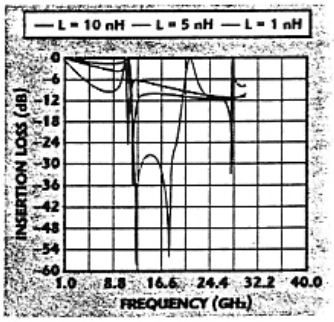

▲ *Fig. 4 The re-entrant filter response in a lowpass configuration.*

Fig. 5 The re-entrant bandpass filter response. ▼

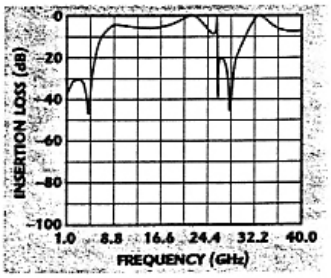

[Continued on page 24]

program used to perform the analysis for the material presented here is much more sophisticated than the program used previously,[1] and contains frequency-dependent enhancements that were not included in the original work. This article explains these enhancements and why they are needed. MATHCAD was used to observe the effects of Z_{ss} values on the filter transfer function, which are shown in ***Figure 6***. The stub and capacitive gap produce the characteristic elliptic function response.

The previous work performed on the re-entrant filter[1] had some limitations. For example, in the value of Z_x of the analysis circuit the capacitive gap was simulated as a simple lumped element in the microstrip line. This method was used to show the effects of a capacitive coupled microstrip line path on the filter response. As a result, the original analysis[1] lacked some subtle effects, which would become more noticeable at higher frequencies or at very low frequencies. This original analysis used the Schuppert model,[5] which assumes perfect coupling for the microstrip-to-slot line junction and produced good results for most cases. However, at lower frequencies the model did not show the coupling degradation that should occur.

The work described in this article has attempted to include some of these effects. In order to obtain higher fidelity from the T-line analysis for a wider spectrum of frequencies, the enhancements to the analysis involve a less-than-perfect microstrip-to-slot line coupling with frequency,[6,7] slot line impedance and wavelength calculation from physical dimensions,[6-9] microstrip impedance and effective dielectric constant,[10] and a microstrip gap model.[6] Other effects, such as those of the slot line bends (mitered or unmitered) and mutual coupling between the microstrip and slot lines, would be difficult to simulate. The effects of imperfect coupling were included by adding an n:1 turns ratio transformer to the Schuppert[5] model in the slot line circuit and slot line stub sections of the model, with the value of n being frequency dependent. This method is a combination of the Schuppert and Knorr transitions[4,5] with Cohn's slot voltage definition.[7] The Schuppert model[5] is a special case when the value of n is equal to 1. Otherwise, the frequency dependency of n is introduced through Equation 2 using Cohn's definition.[6,7] To obtain the coupling value n, the slot line is assumed to be in

▼ *Fig. 6 The re-entrant filter response.*

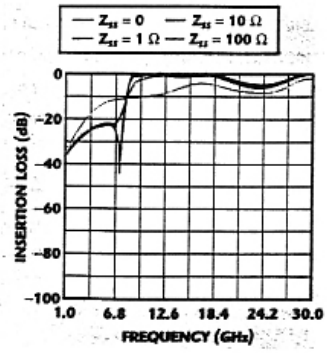

[Continued on page 26]

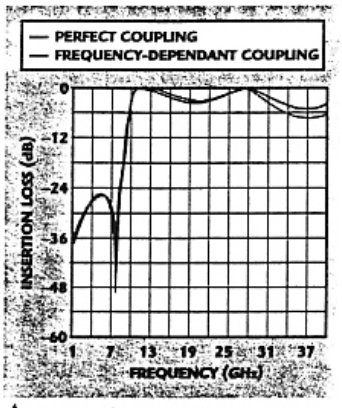

▲ *Fig. 7 A filter response comparison between perfect and imperfect coupling.*

TABLE I
CIRCUIT DIMENSIONS

Item	Measured (")	T-Line (")
l_m	0.0465	0.0390
l_a	0.0906	0.0650
l_s	0.2688	0.2370
W_s	0.081	0.081
W_a	0.018	0.018
S	0.024	0.024
h	0.028	0.028

a cylindrical coordinate system (x, r, ϕ) where x is in the direction of propagation for the slot line. The variable r is the radial direction that will be replaced by h, the ground plane spacing, in the analysis. A field is assumed to exist in the slot line, which can be represented by a magnetic line current source. This magnetic line current would have three far-field components, two magnetic fields (H_x and H_r) and one electric field (E_ϕ). The E_ϕ field decays with distance r and provides a voltage relationship between the slot line voltage (V_s) and the microstrip line voltage (V_m). The transformer turns ratio n is defined as V_m/V_s. The effects of frequency-dependent (less than perfect) coupling compared to the n = 1 case are shown in ***Figure 7***. As expected, the coupling between the lines at the higher frequencies decreases as the fields become more tightly bound to the slot line.

The focus of the work presented here has been directed toward validating the T-line analysis for the reentrant filter. The analysis validation was performed against a prototype circuit and a finite element analysis tool (the HFSS). The physical dimensions of the prototype unit were measured using a measurement microscope and are listed in ***Table 1***.

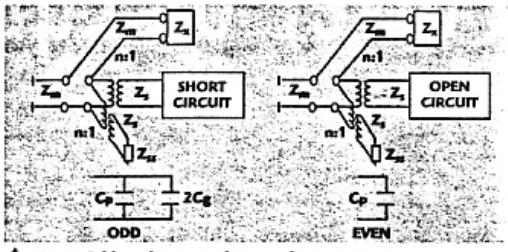

▲ *Fig. 8 Odd- and even-mode equivalent circuits.*

The analysis model reactive impedance Z_x has been replaced with a more elaborate capacitive gap model than the original.[1] The capacitive π network, shown in ***Figure 8***,[6] is used to model the microstrip gap. Most of the published data for this type of microstrip discontinuity are for high dielectric constants ($\varepsilon_r \geq 9$), so slight adjustments had to be made to the capacitive values. The capacitive values for C_p and C_g are computed in the program given the physical dimensions of the gap.

The closed-form equations used for calculating the slot line impedance and wavelength were obtained for $2 \leq \varepsilon_r \leq 9.6$ and $9.7 \leq \varepsilon_r \leq 20$.[6,8] The results from these equations were compared to results obtained using Cohn's method.[7] Cohn used a fictitious waveguide constructed from perfect electrical conducting (PEC) and perfect magnetic conducting walls. Then, the transverse resonance method with a transverse electric (TE) and transverse magnetic (TM) modal expansion was applied to solve for both the impedance and the slot

[Continued on page 28]

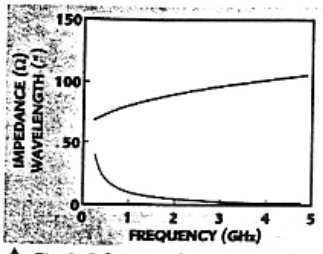

▲ *Fig. 9 Cohn's impedance and wavelength vs. frequency.*

Fig. 10 HFSS simulation vs. measured data. ▼

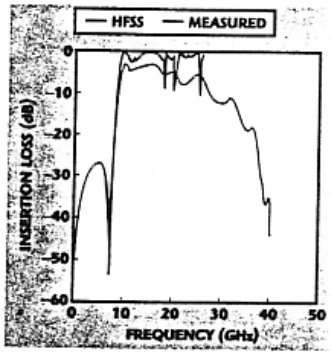

line wavelength. The method was implemented into a MATHCAD program, which computed slot line impedance and wavelength. The equations[6,8] and the results using Cohn's approach agreed closely. The slot line impedance frequency dependence was as expected from a nonpure TEM transmission line, as shown in ***Figure 9***. The cutoff wavelength effect caused by the fictitiously created waveguide can be observed. If a different set of values is used for the analysis, this cutoff effect will change. The analysis program also was fitted with equations to compute microstrip impedance and effective dielectric constant. The closed-form expressions used for this calculation were obtained from Collin.[10]

HFSS was used to analyze the prototype circuit based on the physical dimensions resulting from its dielectric constant ($\varepsilon_r = 2.3$). The HFSS results agreed closely with the measured data and are shown in ***Figure 10***. The prototype was measured initially with SMA connectors on both microstrip ends using a model HP 8510C vector network analyzer, and the data are shown in ***Figure 11***. The HFSS data show some glitches in the response. These glitches are an HFSS-induced artifact due to the PEC enclosure, which was applied to truncate the problem space in HFSS. Although radiation boundary conditions can be used, the size of the analysis would become prohibitive.

As shown in ***Figure 12***, the T-line analysis results also agreed closely with the measured prototype data. The T-line analysis shows that a much wider response could be expected from the filter than was observed from the prototype. Therefore, the SMA connectors were replaced by much higher frequency K connectors. As suspected, the circuit was band limited by the SMA connectors. A significant improvement in bandwidth was achieved with the K connectors. No attempt was made to match the connectors properly to the

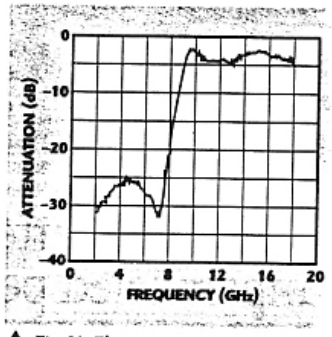

▲ *Fig. 11 The prototype re-entrant filter response.*

Fig. 12 T-line analysis vs. measured and HFSS data. ▼

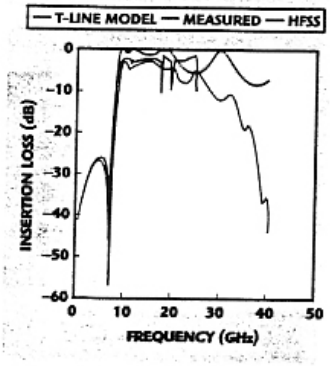

[Continued on page 30]

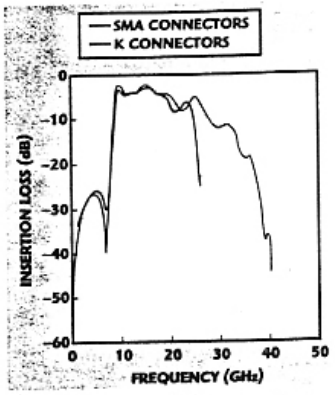

▲ *Fig. 13 A measured data comparison using SMA and K connectors.*

▼ *Fig. 14 Re-entrant filter designations.*

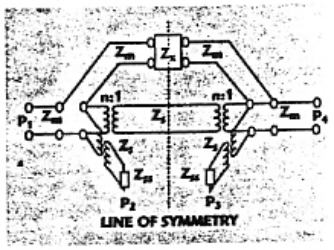

re-entrant circuit. The measured data comparison is shown in ***Figure 13***.

THEORETICAL ANALYSIS

The analysis of the prototype circuit is based on an even-/odd-mode analysis[4] of the T-line circuit, as shown in ***Figure 14***. The variables shown in the circuit are defined as

Z_m = microstrip line impedance
Z_s = slot line impedance
Z_{ss} = slot line stub impedance
Z_{ge} = even-mode impedance of the microstrip gap
Z_{go} = odd-mode impedance of the microstrip gap
Z_{mme} = even-mode impedance of the microstrip circuit
Z_{mmo} = odd-mode impedance of the microstrip circuit
Y_{se} = even-mode admittance of the slot line circuit
Y_{so} = odd-mode admittance of the slot line circuit
l_m = microstrip line length (one side only)
l_s = total slot line length
l_{ss} = slot line stub length
h = ground plane spacing
λ_m = microstrip wavelength
λ_s = slot line wavelength
C_g = series capacitive element
C_p = shunt capacitive element
k_c = slot line propagation constant
n = slot line-to-microstrip coupling V_m/V_s

The equivalent circuit for a microstrip-to-slot line junction has been published by several authors.[2–4,6,7,9] For the purpose of setting up the ABCD matrix equations to analyze the re-entrant circuit, the slot line stub is assumed to be simply a port. The re-entrant filter port definitions are shown. In the general analysis, Z_{ss} is assumed to be a variable impedance that terminates the slot line port. However, Z_{ss} takes on a value of 0 in the analysis and the length of the slot line stub is determined by the desired reject frequency. The even and odd sources are connected to the two microstrip ports (ports 1 and 4) with the line of symmetry, as shown previously. The ABCD matrix coefficients used for the T-line analysis and the equations obtained from the even- and odd-mode equivalent circuits are derived using

$$k_c = j\frac{2\pi}{\lambda_0}\sqrt{\left(\frac{\lambda_0}{\lambda_s}\right)^2 - 1} \quad (1)$$

$$n = \frac{\pi}{2}\left|k_c h H_1^{(1)}(k_c h)\right| \quad (2)$$

even mode:

$$Z_{ge} = \frac{1}{j2\pi f C_p} \quad (3)$$

$$Z_{mme} = Z_m\left(\frac{Z_{ge} + jZ_m\tan(\beta_m l_m)}{Z_m + jZ_{ge}\tan(\beta_m l_m)}\right) \quad (4)$$

$$Y_{se} = j\frac{1}{n^2 Z_s}\tan\left(\frac{2\pi}{\lambda_s}l_s\right) \quad (5)$$

$$\begin{bmatrix} A & B \\ C & D \end{bmatrix}_{EVEN} = \begin{bmatrix} 1 & Z_{mme} \\ 0 & 1 \end{bmatrix}\begin{bmatrix} 1 & 0 \\ Y_{se} & 1 \end{bmatrix}\begin{bmatrix} n & 0 \\ 0 & \frac{1}{n} \end{bmatrix} \begin{bmatrix} \cos(\beta_s l_{ss}) & jZ_s\sin(\beta_s l_{ss}) \\ j\frac{1}{Z_s}\sin(\beta_s l_{ss}) & \cos(\beta_s l_{ss}) \end{bmatrix} \quad (6)$$

$$A_e = n\left(1 + Z_{mme}Y_{se}\right)\cos\left(\frac{2\pi}{\lambda_s}l_{ss}\right) + j\frac{Z_{mme}}{nZ_s}\sin\left(\frac{2\pi}{\lambda_s}l_{ss}\right) \quad (7)$$

$$B_e = jnZ_s\left(1 + Z_{mme}Y_{se}\right)\sin\left(\frac{2\pi}{\lambda_s}l_{ss}\right) + j\frac{Z_{mme}}{n}\cos\left(\frac{2\pi}{\lambda_s}l_{ss}\right) \quad (8)$$

$$C_e = nY_{se}\cos\left(\frac{2\pi}{\lambda_s}l_{ss}\right) + j\frac{nY_{se}}{Z_s}\sin\left(\frac{2\pi}{\lambda_s}l_{ss}\right) \quad (9)$$

$$D_e = jnY_{se}Z_s\sin\left(\frac{2\pi}{\lambda_s}l_{ss}\right) + \frac{1}{n}\cos\left(\frac{2\pi}{\lambda_s}l_{ss}\right) \quad (10)$$

odd mode:

$$Z_{go} = \frac{1}{j2\pi f\left(C_p + 2C_g\right)} \quad (11)$$

$$Z_{mmo} = Z_m\left(\frac{Z_{go} + jZ_m\tan(\beta_m l_m)}{Z_m + jZ_{go}\tan(\beta_m l_m)}\right) \quad (12)$$

$$Y_{so} = \frac{-j}{n^2 Z_s}\cot\left(\frac{2\pi}{\lambda_s}l_s\right) \quad (13)$$

$$\begin{bmatrix} A & B \\ C & D \end{bmatrix}_{ODD} = \begin{bmatrix} 1 & Z_{mmo} \\ 0 & 1 \end{bmatrix}\begin{bmatrix} 1 & 0 \\ Y_{so} & 1 \end{bmatrix}\begin{bmatrix} n & 0 \\ 0 & \frac{1}{n} \end{bmatrix} \begin{bmatrix} \cos(\beta_s l_{ss}) & jZ_s\sin(\beta_s l_{ss}) \\ j\frac{1}{Z_s}\sin(\beta_s l_{ss}) & \cos(\beta_s l_{ss}) \end{bmatrix} \quad (14)$$

$$A_o = n\left(1 + Z_{mmo}Y_{so}\right)\cos\left(\frac{2\pi}{\lambda_s}l_{ss}\right) + j\frac{Z_{mmo}}{nZ_s}\sin\left(\frac{2\pi}{\lambda_s}l_{ss}\right) \quad (15)$$

$$B_o = jnZ_s\left(1 + Z_{mmo}Y_{so}\right)\sin\left(\frac{2\pi}{\lambda_s}l_{ss}\right) + \frac{Z_{mmo}}{n}\cos\left(\frac{2\pi}{\lambda_s}l_{ss}\right) \quad (16)$$

$$C_o = nY_{so}\cos\left(\frac{2\pi}{\lambda_s}l_{ss}\right) + j\frac{nY_{so}}{Z_s}\sin\left(\frac{2\pi}{\lambda_s}l_{ss}\right) \quad (17)$$

$$D_o = jnY_{so}Z_s\sin\left(\frac{2\pi}{\lambda_s}l_{ss}\right) + \frac{1}{n}\cos\left(\frac{2\pi}{\lambda_s}l_{ss}\right) \quad (18)$$

[Continued on page 32]

To obtain the reflection coefficient Γ_e at port P1 with P2 terminated into Z_{ss}, the ABCD matrix definition at P1 is used as

$$\begin{bmatrix} V_1 \\ I_1 \end{bmatrix}_{EVEN} = \begin{bmatrix} A_e & B_e \\ C_e & D_e \end{bmatrix} \begin{bmatrix} V_2 \\ I_2 \end{bmatrix} \quad (19)$$

At P2, V_2 is defined in terms of the terminating impedance Z_{ss} and the current I_2

$$V_2 \equiv Z_{ss} I_2 \quad (20)$$

Substituting for V_2 in Equation 19 yields

$$\begin{bmatrix} V_1 \\ I_1 \end{bmatrix}_{EVEN} = \begin{bmatrix} A_e & B_e \\ C_e & D_e \end{bmatrix} \begin{bmatrix} Z_{ss} I_2 \\ I_2 \end{bmatrix} \quad (21)$$

The equation for the input impedance at P1 is the ratio of V_1 over I_1.

Thus, from Equation 21,

$$Zin_e = \left.\frac{V_1}{I_1}\right|_e = \frac{A_e Z_{ss} + B_e}{C_e Z_{ss} + D_e} \quad (22)$$

From this input impedance and the characteristic impedance (Z_0), the reflection coefficient is given by

$$\Gamma_e = \frac{Zin_e - Z_0}{Zin_e + Z_0} \quad (23)$$

Replacing Z_0 with the characteristic impedance for microstrip Z_m and substituting the ABCD matrix coefficients from the previous equation, the equation Γ_e then becomes

$$\Gamma_e = \frac{A_e Z_{ss} - D_e Z_m + B_e - C_e Z_{ss} Z_m}{A_e Z_{ss} + D_e Z_m + B_e - C_e Z_{ss} Z_m} \quad (24)$$

For the odd-mode case, the equation for Γ_o is derived similarly as

$$\Gamma_o = \frac{A_o Z_{ss} - D_o Z_m + B_o - C_o Z_{ss} Z_m}{A_o Z_{ss} + D_o Z_m + B_o - C_o Z_{ss} Z_m} \quad (25)$$

To obtain the signal flow from port 1 to port 4, the odd-/even-mode coefficients are combined to obtain the signal at P4 as designated by Wheeler.[4] The equation for the signal at port 4 relative to an input at port 1 is herein defined as the transmission coefficient S_{21} for the overall circuit and is given by

$$S_{21} = \frac{1}{2}(\Gamma_e - \Gamma_o) \quad (26)$$

RESULTS

The results of this analysis are compared to the measurements made on the prototype unit and the HFSS results. The prototype's physical dimensions were used in the HFSS and the T-line analysis. These values are in good agreement with each other, which further demonstrates the validity of the analysis. Furthermore, the results are in good agreement with the measured data. Neither the HFSS simulation nor the T-line analysis model included conductor losses although these certainly could be included with minimal work. The results of the T-line analysis and the HFSS solution also were compared and agree closely.

[Continued on page 34]

CONCLUSION

This article shows that relatively accurate results may be obtained for predicting the re-entrant filter response using a simple analysis method. This analysis method also can be used for designing multi-octave filters with a compact geometry. The analysis method has been shown to yield comparable results to those of a finite element model solution with a significant reduction in computational time. Although the results for the analysis show good agreement, additional refinements of the model would further improve the accuracy. Slight differences exist between the physical data and the T-line data due to the effects unaccounted for in the T-line model. These types of effects were noted by other authors originally[5,9] and were accounted for by lengthening or shortening the microstrip and slot line circuits. The improvements include the effects mentioned previously such as slot line bends (mitered or unmitered) for slot lines and parasitic coupling between the microstrip and the slot line. However, obtaining closed-form solutions for these effects is not a trivial task.

ACKNOWLEDGMENT

HFSS is a product of Hewlett-Packard Co., Westlake Village, CA and Ansoft Corp., Pittsburgh, PA. ■

References

1. M.M. Radmanesh and B. Arnold, "Re-entrant Filter Design Uses Microstrip-to-slotline Transitions," *Microwaves & RF*, March 1995, pp. 147–151.
2. M.M. Radmanesh and B. Arnold, "Generalized Microstrip Slot Line Transitions: Theory and Simulation vs. Experiment," *Microwave Journal*, Vol. 36, No. 6, June 1993, pp. 89–95.
3. M.M. Radmanesh and B. Arnold, "Microstrip Slot Line Transitions: Simulation vs. Experiment," IEEE MTT-S International Microwave Symposium, *EEsof Users Group Digest*, June 1992.
4. J. Reed and G. Wheeler, "A Method of Analysis of Symmetric Four-port Networks," *IRE Transactions on Microwave Theory and Techniques*, Vol. MTT-4, October 1956, pp. 246–252.
5. B. Schuppert, "Microstrip Slot Line Transitions: Modeling and Experimental Investigation," *IEEE Transactions Microwave Theory Techniques*, Vol. MTT-36, August 1988, pp. 1272–1282.
6. K.C. Gupta, R. Garg and I.J. Bahl, *Microstrip Lines and Slot Lines*, Artech House Inc., Norwood, MA, 1979.
7. S.B. Cohn, "Slot Line on a Dielectric Substrate," *IEEE Transactions Microwave Theory Techniques*, Vol. MTT-17, October 1969, pp. 768–778.
8. R. Janaswami and D. Schaubert, "Slot Line on Low Permittivity Substrates," *IEEE Transactions Microwave Theory Techniques*, Vol. MTT-34, August 1996, pp. 900–902.
9. J. Knorr, "Slot Line Transitions," *IEEE Transactions Microwave Theory Techniques*, Vol. MTT-22, May 1974, pp. 548–554.
10. R.E. Collin, *Foundations for Microwave Engineering*, Second Edition, McGraw Hill Inc., 1992.